



Sensitivity analysis of an in-plane MEMS vibratory gyroscope

P. Krishna Menon¹ · Jagannath Nayak¹ · Rudra Pratap²

Received: 7 July 2017 / Accepted: 8 December 2017 / Published online: 20 December 2017
© Springer-Verlag GmbH Germany, part of Springer Nature 2017

Abstract

This paper aims to put forward a detailed sensitivity analysis of an in-plane MEMS gyroscope with respect to various performance criteria that are very critical for use of the sensor in different applications ranging from platform stabilization to micro UAVs. Sensitivity analysis involves selecting key design parameters and critical performance criteria and studying the effect of variation of each design parameter on each of the performance criteria. The five key design parameters of the MEMS gyro are the drive stiffness k_d , sense stiffness k_s , drive mass m_d , sense mass m_s and the sense damping coefficient C_s . The four critical gyro performance criteria selected are scale factor, bandwidth, resolution and dynamic range. The influence of variations in different geometric dimensions of the structure on the design parameters of the gyro is also established. The critical geometric dimensions are identified that are then suitably modified allowing faster convergence of the design to meet the desired performance specifications. This study is relevant on two counts (1) the fine tuning of the design to meet all the desired performance criteria with minimum variation in geometric dimensions and with no change in the footprint of the sensor die and (2) the influence of geometric dimensional variations induced during the fabrication of the MEMS gyro structure.

1 Introduction

MEMS vibratory gyroscopes are used to measure the angular rate of a body by sensing the Coriolis force induced motion of the sensing element vibrating in a rotating frame of reference. MEMS gyroscopes find use in a wide variety of applications such as smartphones, automobiles, navigation, bio medical instruments, industrial systems, etc. A considerable amount of research has been done over the past two decades towards the improvement of MEMS gyroscope performance in terms of its scale factor, resolution, dynamic range, temperature sensitivity and bandwidth, with a goal of using them in tactical grade applications (Yoon et al. 2015; Tatar et al. 2014; Tatar et al. 2012; Prikhodko et al. 2011; Trusov et al. 2010; Sharma et al. 2008; Alper et al. 2007; Acar and Shkel 2005, 2009; Kawai et al. 2001; Adamst et al. 1999; Geiger et al. 1999; Park et al. 1997; Tanaka et al. 1995; Bernstein et al. 1993; Blom et al. 1992). The reported studies have

concentrated individually on improving a few performance criteria relevant to the application of interest. For a MEMS gyro to be useful in stabilization applications, it is required to satisfy most of the performance criteria. This necessitates an in depth knowledge of how the fabrication induced geometric tolerances and environmental conditions affect the performance of the MEMS Gyro (Weber et al. 2004; Ferguson et al. 2005; Dong and Xiong 2009). These studies conducted in the sensor design phase can tremendously improve the confidence of the designer in having the fabricated device perform to the design specifications within the tolerance limits.

This paper focusses on the design and simulation of an in-plane MEMS vibratory gyroscope to achieve high performance specifications following a detailed sensitivity analysis of various performance criteria that are critical for its use in different applications ranging from platform stabilization to micro UAVs. The performance criteria such as scale factor, bandwidth, resolution and dynamic range are known in terms of lumped structural parameters such as drive stiffness (k_d), sense stiffness (k_s), drive mass (m_d), sense mass (m_s) and sense damping coefficient (C_s). In order to achieve the target performance of a gyro, it is, therefore, easier to seek optimum values of these lumped parameters with minimum possible iterations. Unfortunately, the lumped parameters are not the direct design

✉ P. Krishna Menon
krishna.menon@rcilab.in; kmenonp@gmail.com

¹ Research Centre Imarat, Hyderabad 500 069, India

² Centre for Nanoscience and Engineering, Indian Institute of Science, Bangalore 560 012, India

variables that a designer can pick. These parameters, in turn, depend on the geometric dimensions and material properties of the structure. Thus we have a two-step mapping as shown in Fig. 1 while designing for a given performance specification. It is also clear from Fig. 1 that each of the two steps in this design process is an exercise in multidimensional mapping. Conceptually, it is possible to carry out this multi-step optimization but the computational effort will be enormous. In this work, we propose and show an approach that requires much less effort to achieve the target specifications. Our approach is based on calculations of sensitivities of the performance criteria with respect to the lumped parameters, and identification of independent parameters. We start with an initial design configuration of the gyro (much like an educated guess for initial values in any iterative process) and show how the sensitivity analysis helps us in converging to the right design parameters with one or two design iterations in order to meet the desired performance specification. Finally, the technique of choosing the most appropriate design parameters and corresponding geometric dimensions is demonstrated using case studies. Here we must point out that the idea and the method of sensitivity analysis used here is not new; however, its application in gyroscope design is new. Most of the work reported in the literature uses ad-hoc approaches to reach a design configuration. In the present work, we derive expressions for most relevant design sensitivities and show how they help in reaching target specifications very quickly.

2 MEMS gyroscope design configuration

The basic design configuration of the MEMS gyroscope is selected from the work of Mochida et al. (2000) because of the Z-axis sensing configuration with independent beams for the drive and sense modes. This leads to negligible cross coupling between the drive and sense modes, low quadrature error and hence low bias stability. The g effects can be nullified using dual proof mass configuration with differential sensing. The published value of resolution is $0.07^\circ/s$ with a bandwidth of 10 Hz. The initial structural dimensions are shown in Table 1 and the basic structure is shown in Fig. 2. It may be noted that the far ends of the drive beams are anchored in place. The drive beam length

Table 1 Structural dimensions of the basic design

Structural dimension	Value (μm)
Structure thickness (d_t)	58
Sense beam width (w_s)	11
Sense beam thickness (d_s)	8
Drive beam length (l_d)	700
Drive beam width (w_d)	8
Sensing gap (g_0)	5

mentioned is the length of the longer beam and the length of the shorter beam is kept constant at 300 μm .

These dimensional values give rise to the following nominal values of design parameters listed in Table 2.

3 Modelling and simulation

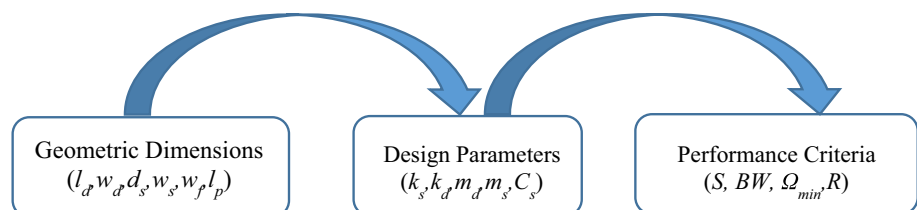
3.1 3D modelling of the basic MEMS gyro structure

The material properties of Si (100) with orthotropic Young's Modulus are used for simulation. The values are taken from the literature (Hopcroft et al. 2010). The 3D model of the structure as seen in Coventor MEMS+ software is shown in Fig. 3. The fabrication process of the structure uses a highly conductive SOI wafer with the required device layer thickness. The device layer is deep reactive-ion etched (DRIE) from the front side using a mask and then bonded to a glass wafer. The carrier layer is removed and the Silicon device layer is deep reactive-ion etched from the back side using another mask to release the sense beams and other parts of the structure. This stack is then bonded to a top glass cover wafer to encapsulate the sensor structure at the required pressure. The top and bottom glass wafers carry the necessary electrodes and metal pattern for driving and sensing.

3.2 Modal analysis

The modal analysis of the structure is carried out to determine the drive and sense modes of the gyroscope. The first mode of in-plane oscillations is the drive mode of the structure as shown in Fig. 4a and the first mode of out-of-

Fig. 1 The two-step mapping process



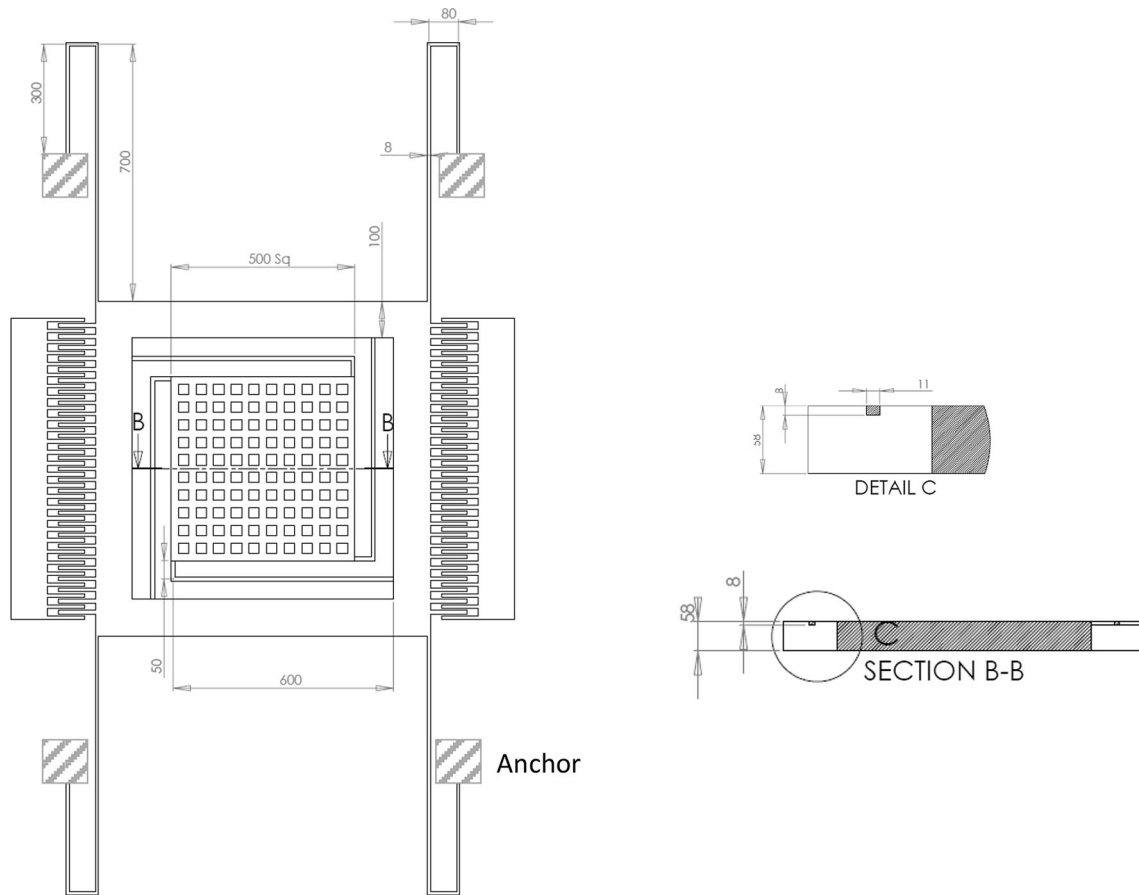


Fig. 2 2D views of the structure

Table 2 Nominal values of design parameters

Design parameter	Values
Drive stiffness (k_d)	35.39 N/m
Sense stiffness (k_s)	11.28 N/m
Drive mass (m_d)	7.5×10^{-8} kg
Sense mass (m_s)	2.34×10^{-8} kg
Sense damping coefficient (C_s)	3.33×10^{-6} N/(m/s)

plane oscillations is the sense mode of the structure as shown in Fig. 4b. The Q-factors and the equivalent masses can be extracted from this analysis.

3.3 Damping analysis

The damping analysis of the structure is carried out using Coventorware software. The squeeze film damping coefficient variation with frequency is analysed taking into consideration only the perforated proof mass and neglecting the contribution of the sense beams owing to their very small width and large gap from the substrate. The plot is

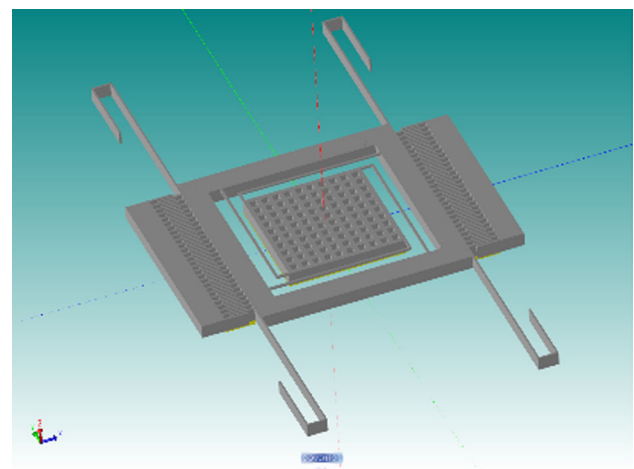


Fig. 3 3D model of the structure

shown in Fig. 5a. The slide film damping coefficient is calculated considering all the comb-finger pairs and the proof mass with frame motion over the sensing electrode during the drive mode. The frequency variation of the slide film damping coefficient is shown in Fig. 5b. As expected, the slide film damping coefficient is an order of magnitude

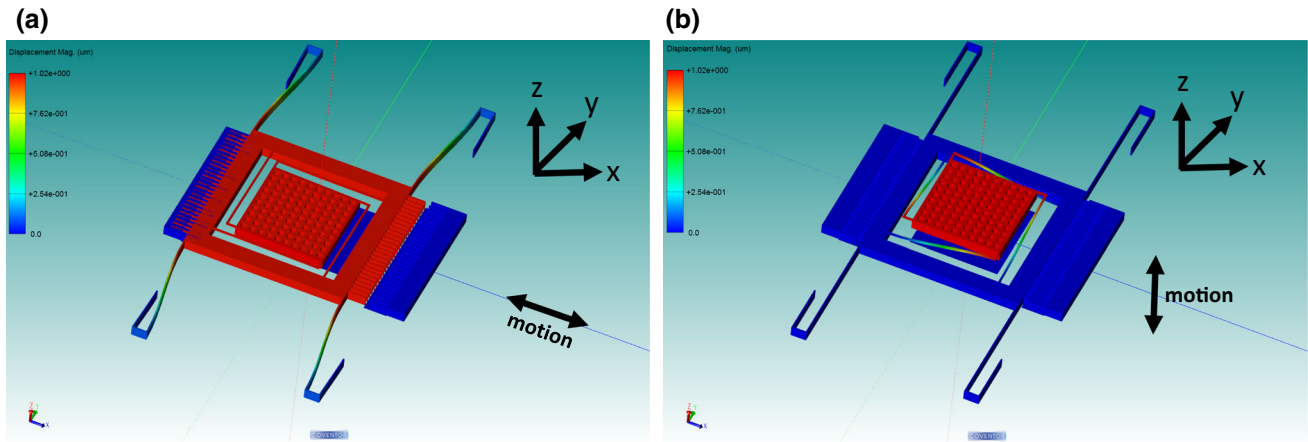


Fig. 4 a Mode 1—drive mode: 3457 Hz; b mode 2—sense mode: 3495 Hz

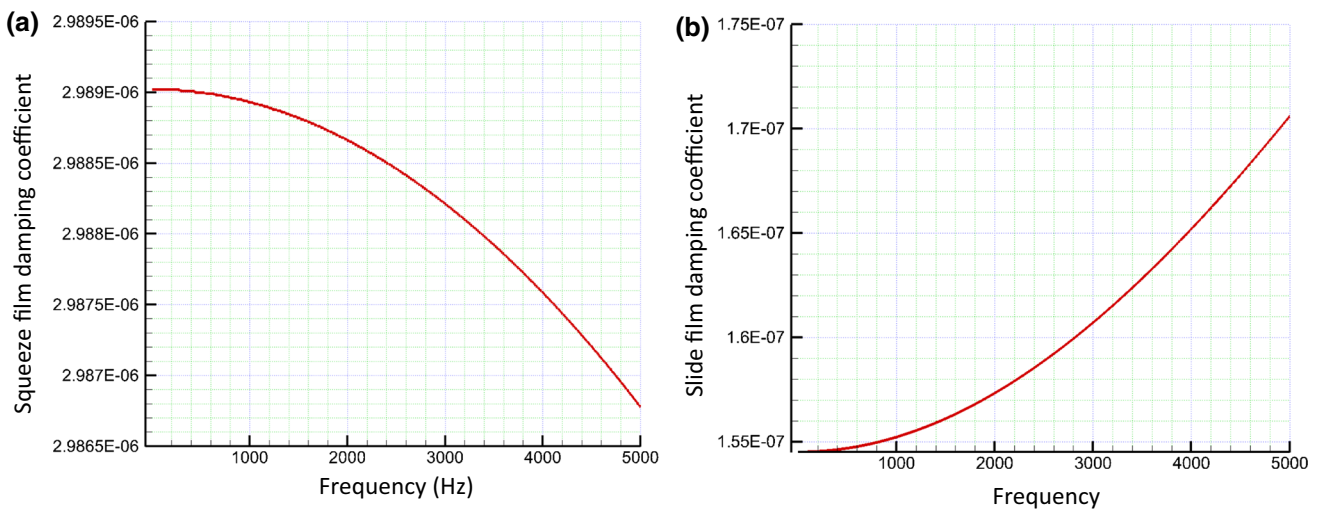


Fig. 5 a Squeeze film damping coefficient variation with frequency; b slide film damping coefficient variation with frequency

smaller than the squeeze film damping coefficient (Senturia 2001).

The values of the total damping coefficients for each mode ($c_{resonance1}$ and $c_{resonance2}$) are calculated and they are used to compute the equivalent material damping coefficients as given in literature (Coventor Inc 2015; Chang et al. 2010). These values are used for further simulations.

$$\alpha = 2\omega_1\omega_2 \frac{(\zeta_1\omega_2 - \zeta_2\omega_1)}{\omega_2^2 - \omega_1^2} \tag{1}$$

$$\beta = 2 \frac{(\zeta_2\omega_2 - \zeta_1\omega_1)}{\omega_2^2 - \omega_1^2}, \tag{2}$$

where $\zeta_1 = \frac{c_{resonance1}}{2m_1\omega_1}$ and $\zeta_2 = \frac{c_{resonance2}}{2m_2\omega_2}$ are the damping ratios of the first and second mode respectively. Here α and β are the mass dependent and spring dependent material damping coefficient respectively. ω_1 and ω_2 are the first and second modal frequencies of the structure, and m_1 and m_2 are equivalent drive and sense masses respectively.

3.4 Coupled AC and DC analysis

The coupled AC and DC analysis is carried out for several DC voltages ranging from 2 to 25 V keeping AC voltage fixed at $V_{AC} = 5$ V. In order to get a maximum displacement of approximately 15 μm (one third the gap between the comb tip and anchor which is 45 μm in this case), the voltage required is found to be $V_{DC} = 18$ V. The maximum drive displacement in the X-direction is 14.61 μm . The resonant peak corresponding to the drive mode is obtained at a frequency of 3457 Hz as shown in Fig. 6.

3.5 Coriolis displacement and 'g' effect

The coupled AC and DC analysis with angular rate in the Y-direction is carried out to find the Coriolis displacement of the sense mass in the Z-direction at different angular

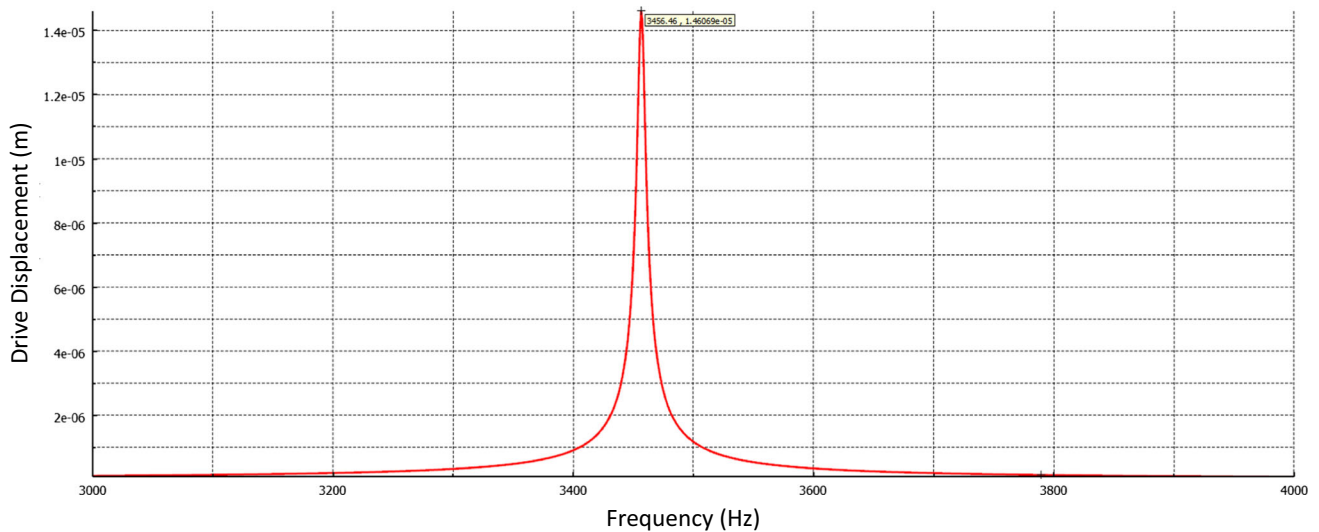


Fig. 6 Maximum drive displacement

rates. The angular rate is varied from 0 to 400°/s in steps of 50°/s. The maximum Coriolis displacement for an angular rate of 400°/s is 424 nm (Fig. 7). Here the total sense gap is 5 μm.

The g-effect is studied by applying 1 g acceleration along X, Y and Z directions when the structure is driven in X direction and angular rate is applied in Y direction. The peak Coriolis displacement is then observed for any change from 0 g condition. The g-effect is found to be maximum when the acceleration is applied along the X-direction. This is because of large drive displacement and hence more Coriolis force acting on the proof mass. This can be cancelled by using dual proof mass structure driven out of phase.

3.6 Thermal effect

Modal analysis is carried out at different temperatures ranging from − 40 to + 80 °C in steps of 20 °C and the change in modal frequencies is studied. It is seen that the drive frequency decreases with increase in temperature as shown in Fig. 8. This is because of the longer and thicker U-shaped beams which results in a larger change in the in-plane drive frequency with temperature. The sense frequency is found to be almost constant in the temperature range because of the shorter and thinner L-shaped beams which results in a smaller change in the out of plane sense frequency with temperature. For a fixed drive frequency, the Coriolis displacement is found to decrease as a result of the decreased drive displacement as the resonance peak

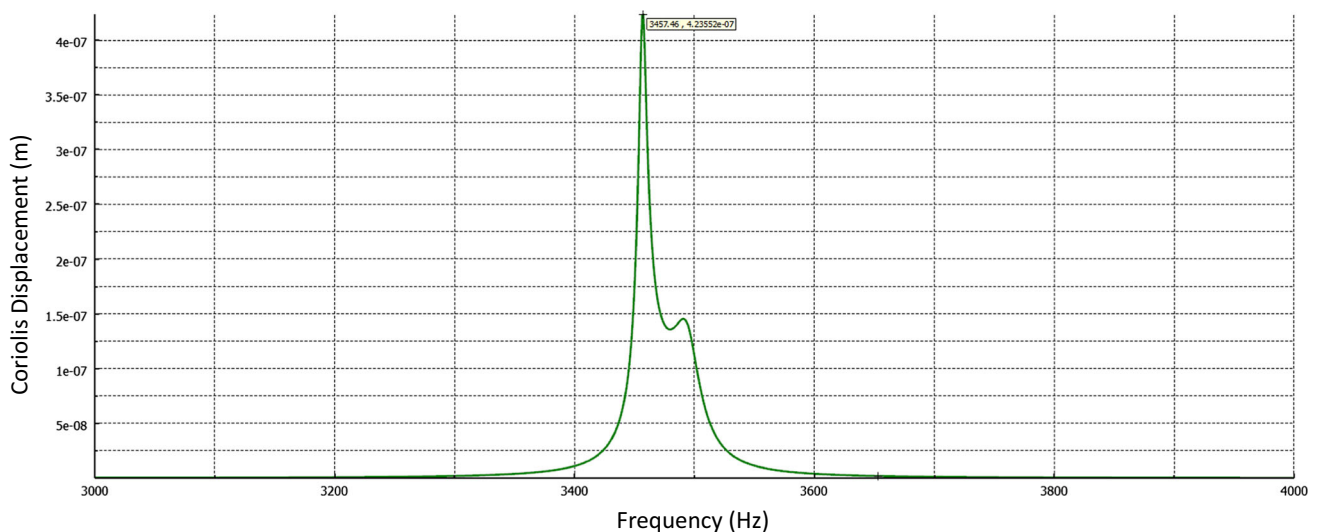


Fig. 7 Coriolis displacement of the sense mass for the maximum angular rate of 400°/s

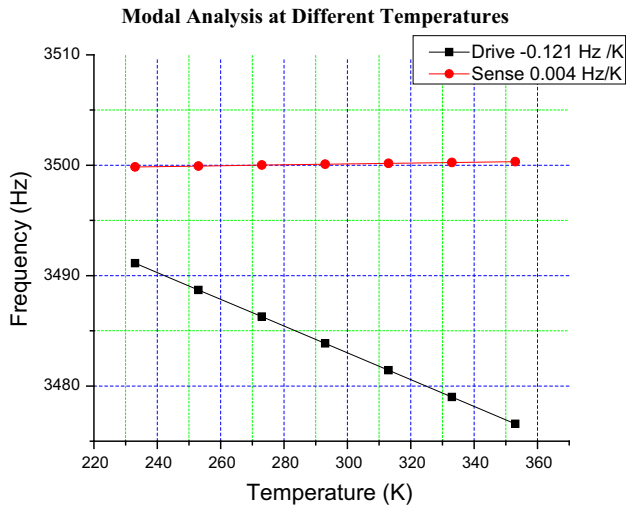


Fig. 8 Modal analysis at different temperatures

keeps shifting to the lower side with increase in temperature. This can be easily compensated later by keeping the drive amplitude constant using the automatic gain of the control loop in the drive circuit of the Gyro ASIC.

3.7 Thermomechanical noise

The resolution of the MEMS gyroscope is limited by the thermomechanical noise. The thermal noise equivalent rate signal Ω_n is given by (Bao 2000),

$$\Omega_n = \sqrt{\frac{k_B T \omega_2 \Delta f}{m \omega_1^2 A_1^2 Q_2}} \tag{3}$$

where k_B is the Boltzmann constant, T is the ambient temperature, ω_2 is the sense mode resonant frequency, Δf is the bandwidth, m is the sense mass, ω_1 is the drive frequency, A_1 is the drive displacement and Q_2 is the sense quality factor. Plugging in the values, we get the Thermomechanical Noise Equivalent Rate (TNER) as $\Omega_n = 0.0045^\circ/s$ at 300 K. The maximum value of Ω_n corresponds to the maximum operational temperature of 353 K, and it is $0.0049^\circ/s$. These values define the noise floor for the gyro.

3.8 Bandwidth

The transient analysis of the MEMS gyroscope is carried out using MEMS+ and Simulink interface. The schematic is as shown in Fig. 9a. The output shows the drive displacement, sense displacement and input angular rate signal at a frequency of 20 Hz (Fig. 9b). The 3 dB bandwidth is found to be about 27.5 Hz.

3.9 Scale factor

The sense displacement of the MEMS gyroscope is plotted against the applied angular rate in Fig. 10a. The slope of this line gives the value of the scale factor in terms of the Coriolis displacement and is found to be $1.06 \text{ nm}/(^\circ/s)$. The sense capacitance is also plotted against the applied angular rate in Fig. 10b. The slope of this line gives the scale factor as $0.1416 \text{ fF}/(^\circ/s)$.

The analytical expression for the scale factor or rate sensitivity in terms of Coriolis displacement is (Bao 2000),

$$S = \frac{2A_d \omega_d}{\omega_s^2 \sqrt{\left(1 - \frac{\omega_d^2}{\omega_s^2}\right)^2 + \frac{C_s^2 \omega_d^2}{m_s^2 \omega_s^4}}} \tag{4}$$

where the drive frequency $\omega_d = \sqrt{\frac{k_d}{m_d}}$, sense frequency $\omega_s = \sqrt{\frac{k_s}{m_s}}$, A_d is the drive displacement and C_s is the sense damping coefficient and thus $S = S(k_d, k_s, m_d, m_s, C_s)$.

After plugging in the values of different variables, the analytical scale factor is found to be $1.03 \text{ nm}/(^\circ/s)$ which is very close to the simulated value of $1.06 \text{ nm}/(^\circ/s)$. In terms of change in capacitance, the value of the scale factor is $0.1416 \text{ fF}/(^\circ/s)$ in differential mode.

3.10 Resolution

From the simulated sensitivity value of $141.6 \text{ aF}/(^\circ/s)$, the resolution of $0.0071^\circ/s$ is obtained assuming that the minimum measurable capacitance is 1 aF . The analytical value of resolution for differential capacitive measurement from a single proof mass is calculated using the following equation (Apostolyuk 2006)

$$\Omega_{\min} = \frac{\Delta C_{\min} g_0^2}{2 \epsilon_0 A S} \tag{5}$$

where $\Delta C_{\min} = 1 \text{ aF}$ is the minimum measurable capacitance, g_0 is the gap between the proof mass and the sense electrode, ϵ_0 is the dielectric constant of air, A is the sensing area of the proof mass and S is the sensitivity in $\text{m}/(^\circ/s)$. The analytically computed value is $0.0055^\circ/s$ which is close to the simulated value. Taking into account the value of TNER also, the resolution can be approximated as $0.01^\circ/s$ for a minimum detectable capacitance of 1 aF .

3.11 Dynamic range

The dynamic range of the angular rate sensor is given by Apostolyuk (2006),

$$R = 20 \times \log_{10} \left(\frac{\Omega_{\max} - \Omega_{\min}}{\Omega_{\min}} \right) \tag{6}$$

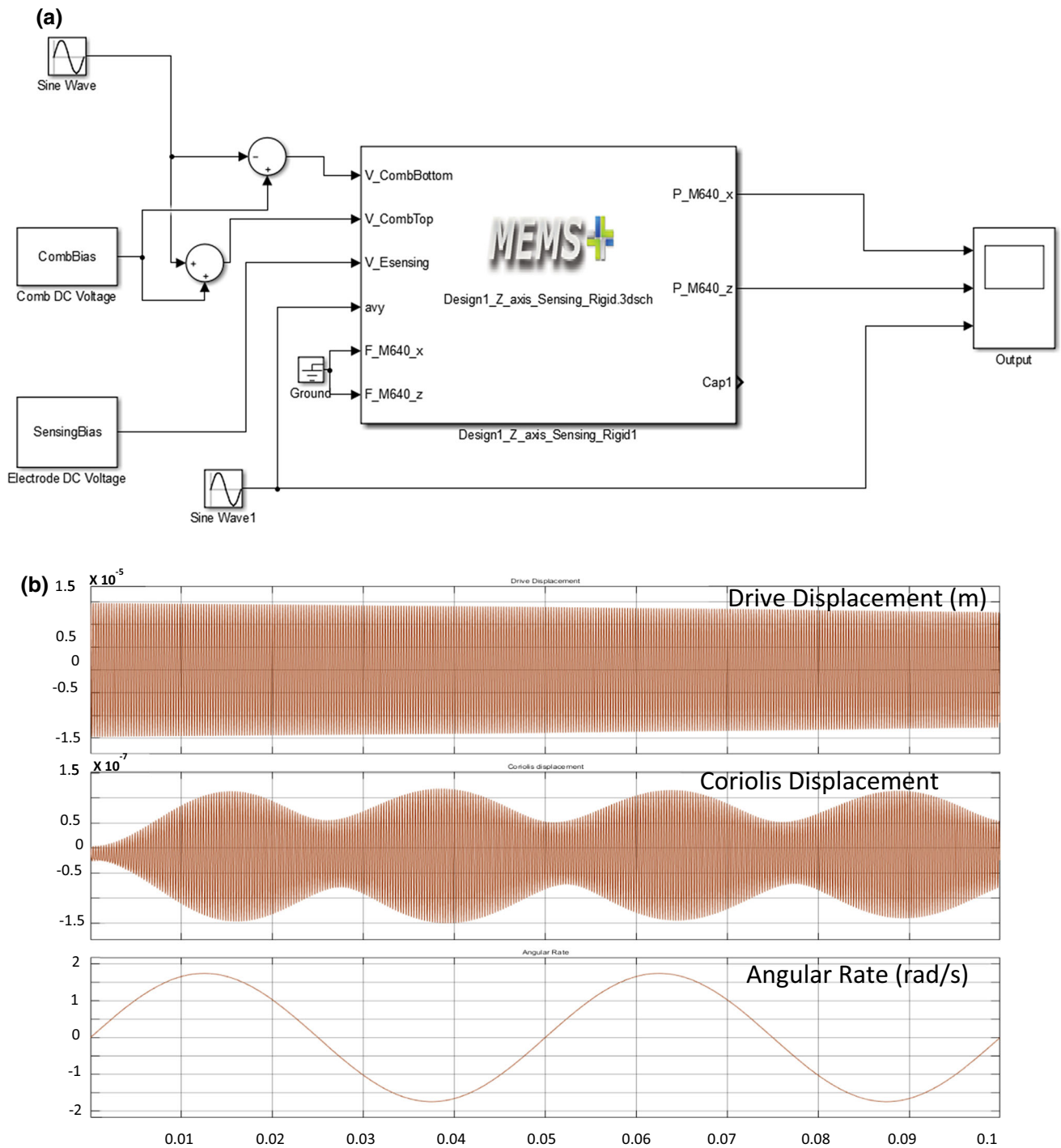


Fig. 9 a Schematic of the SIMULINK model for transient analysis; b simulation results

where Ω_{max} is the maximum angular rate for the full scale output and Ω_{min} is the resolution of the Gyro.

For a targeted maximum angular rate of $\Omega_{max} = 400^\circ/s$ and $\Omega_{min} = 0.01^\circ/s$, the dynamic range is approximately 92 dB. The final performance specifications of the designed MEMS gyroscope are given in Table 3.

4 Sensitivity analysis

The sensitivity analysis involves the study of the effect of variation in each of the design parameters on the critical performance criteria of the MEMS gyro. The five key design parameters are drive stiffness (k_d), sense stiffness (k_s), drive mass (m_d), sense mass (m_s) and sense damping

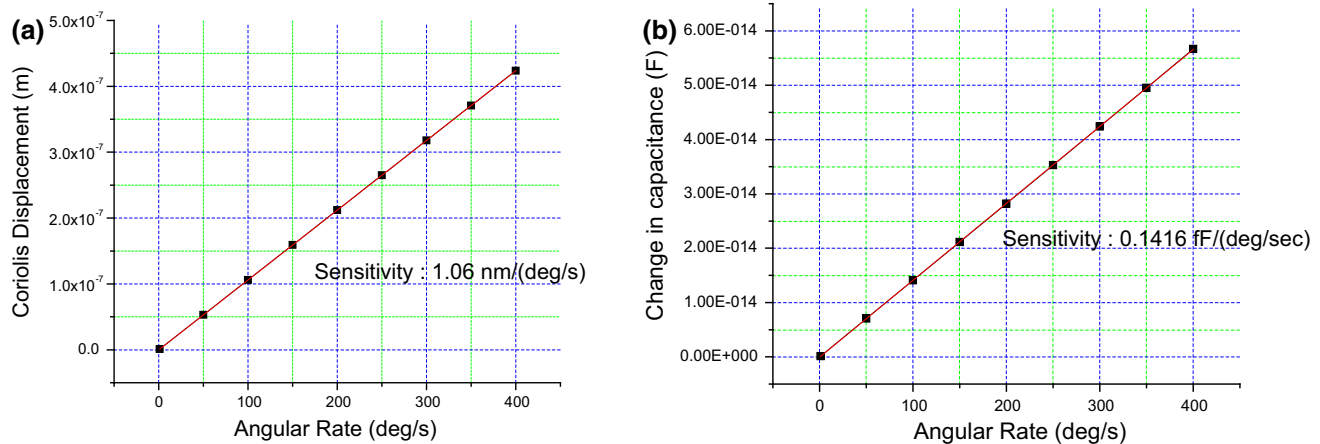


Fig. 10 **a** Coriolis displacement at different angular rate; **b** sense capacitance at different angular rates

Table 3 Performance criteria of MEMS gyroscope

Performance criteria	Value
Scale factor (S)	0.1416 fF/(°/s)
Resolution (Ω_{\min})	0.01°/s
Dynamic range (R)	92 dB
Bandwidth (BW)	25 Hz
g effect (max in 3 directions)	0.27 (°/s)/g
Thermomechanical noise @ 300 K	0.00454°/s

coefficient (C_s). The four critical performance criteria are scale factor, bandwidth, resolution and dynamic range. This analysis helps in reducing the laborious design trials required for achieving the desired high performance specifications.

4.1 Mutual dependence of the design parameters

The design parameters are varied by changing the respective geometric dimensions of the structure. While selecting the geometric dimensions to vary, care is taken to pick those dimensions which when varied have the least effect on other design parameters. The drive stiffness (k_d) is varied by changing either drive beam length (l_d) or drive beam width (w_d). Sense stiffness (k_s) is varied causing least effect on other design parameters by changing the sense beam thickness (d_s) or sense beam width (w_s). Drive mass (m_d) is varied by changing the width of the frame (w_f) and sense mass (m_s) by varying the size of the proof mass (l_p). Damping coefficient (C_s) is varied by changing the gas pressure of the medium between the proof mass and the substrate. It is very important to study the effect of change in one design parameter on others. This will help the designer to

independently vary one particular geometric dimension to achieve change in the corresponding design parameter with least effect on other design parameters.

Table 4 shows the magnitude of change in each design parameter when the respective geometric dimensions are varied and also the effect of this change on other design parameters. Each of the above geometric dimension is varied around $\pm 10\%$ assuming process variations to the critical dimension (CD) patterned on a wafer. The overall structural thickness except the sense beam part is decided by the device layer thickness of the SOI wafer and this is kept constant for all simulations.

It is apparent from Table 4 that changing the drive beam width (w_d) has more effect on k_d and negligible effect on other design parameters ($< 1\%$). For changing k_s , the thickness of the sense beam (d_s) is the most appropriate geometric parameter as a change in d_s leads to an almost independent variation of k_s . Thus we can conclude that for varying the design parameters k_d , k_s , m_d , m_s and C_s , we can select the geometric dimensions as w_d , d_s , w_f , l_p and $P_{damping}$ respectively. It may be noted that a 10% change in ambient pressure does not contribute much to the value of sense damping coefficient C_s .

4.2 Effect of variation in k_d , k_s , m_d , m_s and C_s on scale factor

The scale factor or the rate sensitivity of the gyro is given by Eq. (4) where the dependence of the scale factor on the design parameters k_d , k_s , m_d and m_s is implicit through ω_d and ω_s . The dependence of scale factor on drive stiffness k_d is analysed by computing the partial derivative of S with respect to k_d .

Table 4 Dependence of design parameters on geometric dimensions of the structure

Design parameter	Geometric dimension being varied	Percentage change in other design parameters				
		k_d	k_s	m_d	m_s	C_s
k_d	l_d (+ 70 μm or + 10%)	- 22.2	- 0.1	0.5	0.4	-
	w_d (-1 μm or - 12.5%)	- 32.5	- 0.2	0.4	0.4	-
k_s	d_s (+ 1 μm or + 12.5%)	0.5	39.6	0.5	0.4	-
	w_s (+ 1 μm or + 9.1%)	0.3	10.1	0.3	0.4	-
m_d	w_f (+ 20 μm or + 10%)	0.2	0.0	6.7	0.0	-
m_s	l_p (- 50 μm or - 10%)	0.3	0.3	- 5.5	- 17.9	-
C_s	$P_{damping}$ (+ 0.1 mbar or + 10%)	-	-	-	-	2.4

$$\frac{\partial S}{\partial k_d} = \frac{1}{2 \times \sqrt{m_d k_d}} \times \left[\frac{2A_d}{\omega_s^2 \sqrt{\sigma_1}} - \left\{ \frac{A_d \omega_d \left[\frac{4\omega_d \left(\frac{\omega_d^2}{\omega_s^2} - 1 \right) + \frac{2\omega_d C_s^2}{m_s^2 \omega_s^4} \right]}{\omega_s^2 \sigma_1^{\frac{3}{2}}} \right\} \right], \tag{7}$$

where $\sigma_1 = \left(\frac{\omega_d^2}{\omega_s^2} - 1 \right)^2 + \frac{\omega_d^2 C_s^2}{m_s^2 \omega_s^4}$

For the designed MEMS gyroscope, the effect of variation in the drive stiffness on scale factor due to change in k_d up to 10% from the nominal value is shown in Fig. 11. As the value of k_d is increased from the nominal value, the sensitivity shoots up to a maximum value and the corresponding value of k_d is obtained for which the slope becomes zero. For further increase in k_d , the sensitivity decreases with a negative slope. It is apparent that beyond 10% variation in k_d from the nominal value, the sensitivity falls by an order of magnitude. This is because the scale

factor depends critically on ω_d and ω_s being close to each other.

The plot of $\frac{\partial S}{\partial k_s}$, $\frac{\partial S}{\partial m_d}$ and $\frac{\partial S}{\partial m_s}$ with respect to the respective normalized design parameters also follow similar pattern.

The dependence of the scale factor on the sense damping coefficient (C_s) is given by Eq. (8). For the designed MEMS gyroscope, the effect on scale factor due to wide variation in the sense damping coefficient is shown in Fig. 12. The plot can be analysed in two separate regions. The region I corresponds to the case when C_s is very small and hence the term involving C_s^2 can be neglected in Eq. (8). We can get maximum scale factor till the value of C_s is approximately three times the nominal value. This is because, the damping has no effect in this region and the rate sensitivity of the gyro is determined only by the separation between the drive and sense frequencies. For higher values of C_s represented by region II, the scale factor is found to reduce slowly as the C_s^2 term in the denominator becomes more and more dominant. Hence we can conclude here that the damping pressure need to be under control so that the value of C_s does not cross more than three times the nominal value. In other words, this corresponds to the

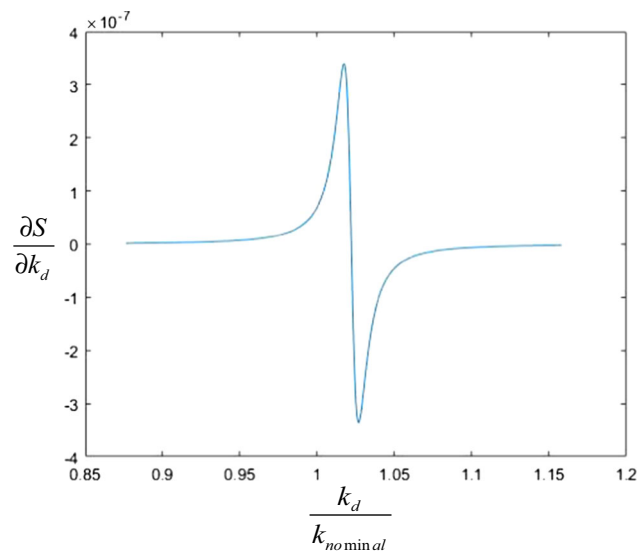


Fig. 11 Effect of variation of drive stiffness on scale factor

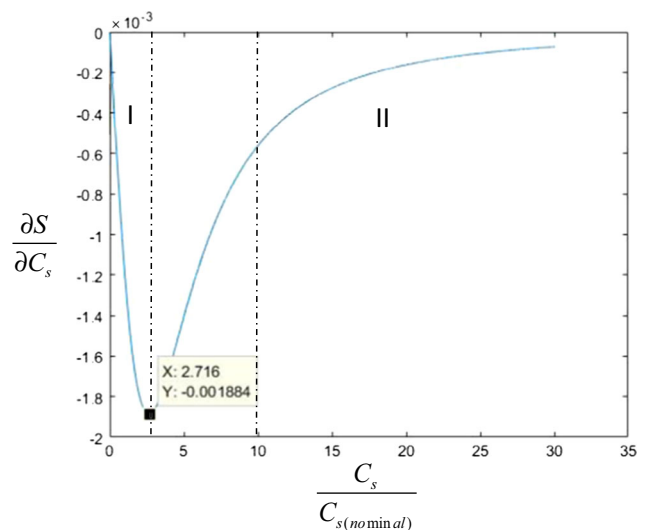


Fig. 12 Effect of variation of damping coefficient on scale factor

case of approximately 50 times increase in damping pressure ($P_{damping}$) from the nominal value of 1 mbar.

$$\frac{\partial S}{\partial C_s} = - \left\{ \frac{2A_d \omega_d^3 C_s}{m_s^2 \omega_s^6 \left[\left(\frac{\omega_d^2}{\omega_s^2} - 1 \right)^2 + \frac{\omega_d^2 C_s^2}{m_s^2 \omega_s^4} \right]^{\frac{3}{2}}} \right\} \quad (8)$$

4.3 Effect of variation in k_d , k_s , m_d , m_s and C_s on bandwidth

The amplitude variation of Coriolis displacement with respect to the frequency of the angular rate is given by the following equation (Bao 2000)

$$A(\omega_s) = \frac{A_d \Omega_0 \omega_d}{\omega_y \Delta \omega \sqrt{4 \left(1 - \frac{\omega_s}{\Delta \omega} \right)^2 + \frac{1}{Q_i^2}}} \times \left\{ 1 + \frac{\left(1 - \frac{\omega_s}{\Delta \omega} \right)^2 + \frac{1}{4Q_i^2}}{\left(1 + \frac{\omega_s}{\Delta \omega} \right)^2 + \frac{1}{4Q_i^2}} + \frac{4 \left(1 - \frac{\omega_s}{\Delta \omega} \right)}{\sqrt{4 \left(1 - \frac{\omega_s}{\Delta \omega} \right)^2 + \frac{1}{Q_i^2}}} \right\}^{\frac{1}{2}} \quad (9)$$

where effective quality factor $Q_i = \frac{\Delta \omega}{\omega_y} Q_y$, $\Delta \omega$ is the difference between the drive and sense frequencies, ω_y is the sense frequency, Q_y is the sense quality factor and ω_s is the frequency of the input angular rate signal. The dependence of the Coriolis displacement (normalized with

respect to the value at constant angular rate) on the frequency of the input angular rate is plotted in Fig. 13a. The 3 dB bandwidth for the present MEMS gyro design is found to be 25 Hz. This closely matches with the system level simulations using MEMS+ Simulink discussed in Sect. 3.8.

The expression for the 3 dB bandwidth given in the literature (Bao 2000), $\Delta \omega_{BW} = 0.54 \times \Delta \omega$ is valid only for $\omega_s \ll \Delta \omega$. From the frequency response studies, we can get the new expression valid for the present case as

$$\Delta \omega_{BW} = 0.6534 \times \Delta \omega \quad (10)$$

where $\Delta \omega = \omega_y - \omega_d$ is the difference between the sense and drive frequencies.

The dependence of bandwidth on design parameters is studied using Eq. (10). For the designed MEMS gyroscope, the effect on bandwidth due to 10% variation in drive stiffness around the nominal value is analysed. The variation is found to be linear with a negative slope. From the plot, we can easily find out the value of the drive stiffness (k_d) below which we can get a non-zero bandwidth. A similar kind of variation is seen with sense mass m_s also. The variation of bandwidth with respect to sense stiffness (k_s) and drive mass (m_d) is found to be linear with a positive slope. From the plots, we can find out the value of design parameters above which a non-zero bandwidth can be obtained. The plot shown in Fig. 13b gives an idea about the variation of bandwidth

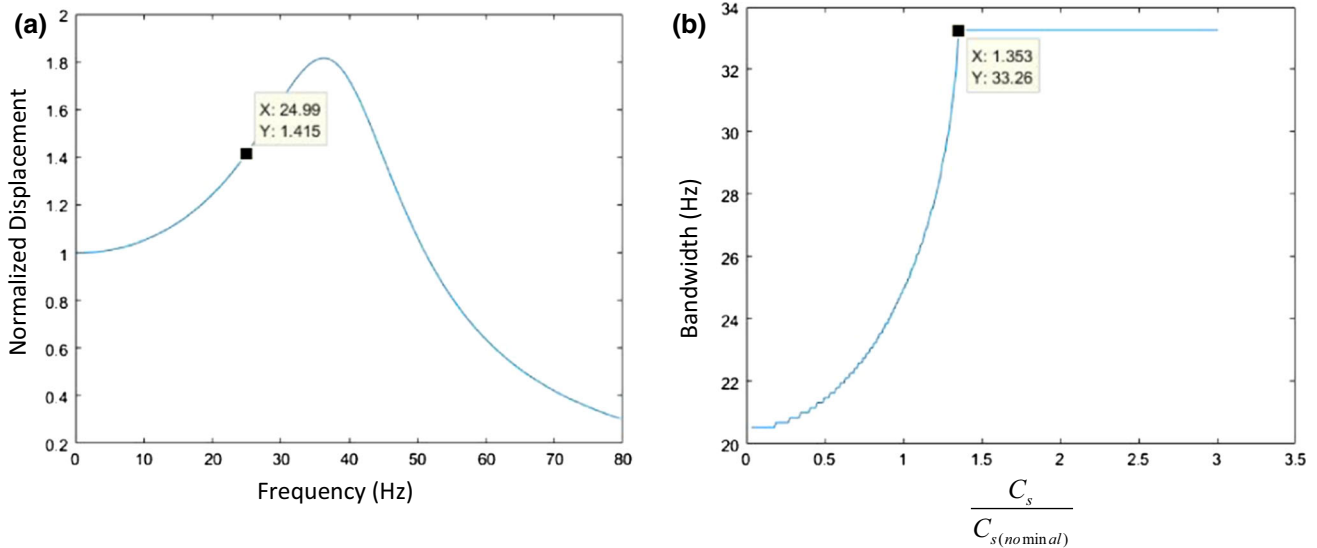


Fig. 13 **a** Frequency response of Coriolis displacement normalized w.r.t the value at constant angular rate; **b** variation of bandwidth with damping coefficient

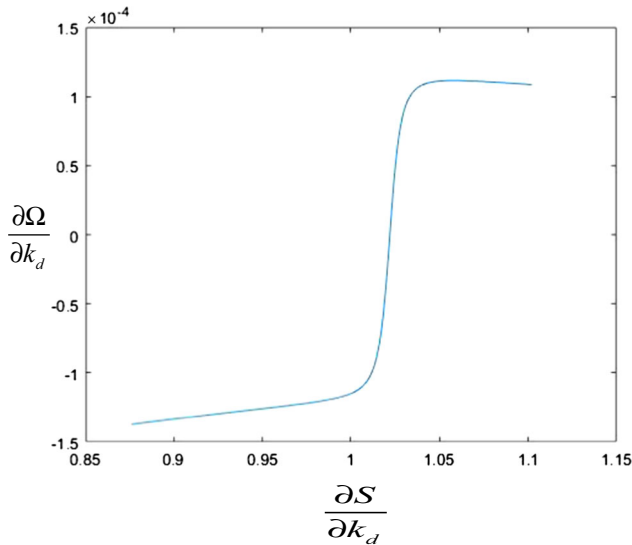


Fig. 14 Effect of variation of drive stiffness on resolution

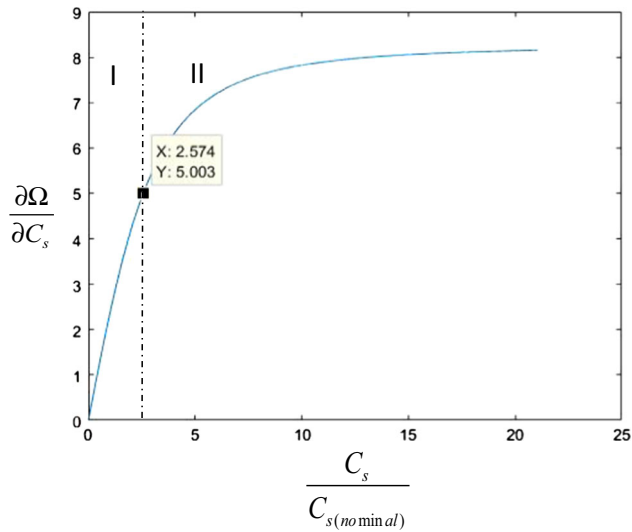


Fig. 15 Effect of variation of damping coefficient on resolution

corresponding to change in damping coefficient. It is observed that the 3 dB bandwidth continuously increases with increase in C_s until it reaches to about 1.35 times the nominal value. This corresponds to the maximum bandwidth of 33 Hz that can be achieved with the given design. For higher values of C_s , the amplitude of Coriolis displacement falls drastically with decrease in the effective sense quality factor Q_i . This corresponds to the over damped region which has no significance to the working of the gyro.

4.4 Effect of variation in k_d , k_s , m_d , m_s and C_s on resolution

The dependence of resolution on drive stiffness k_d , is studied using Eqs. (5) and (10)

$$\frac{\partial(\Omega_{\min})}{\partial k_d} = \frac{-1}{S^2} \times \left(\frac{\Delta C_{\min} g_0^2}{2 \in_0 A} \right) \times \left(\frac{1}{2 \times \sqrt{m_d k_d}} \times \left[\frac{2A_d}{\omega_s^2 \sqrt{\sigma_1}} - \frac{A_d \omega_d \left[\frac{4\omega_d \left(\frac{\omega_d^2}{\omega_s^2} - 1 \right) + \frac{2\omega_d C_s^2}{m_s^2 \omega_s^4} \right]}{\omega_s^2 \sigma_1^{\frac{3}{2}}} \right] \right) \quad (11)$$

where $\sigma_1 = \left(\frac{\omega_d^2}{\omega_s^2} - 1 \right)^2 + \frac{\omega_d^2 C_s^2}{m_s^2 \omega_s^4}$.

The same is plotted with respect to the normalized values of the drive stiffness (k_d) in Fig. 14. The highest resolution corresponds to the value of k_d for which the slope becomes zero. With increase in k_d from the nominal value, the scale factor or rate sensitivity of the gyro S increases, resolution increases, attains a maximum and then it is found to increase almost linearly. The values of k_d for which we can get maximum sensitivity can also give the highest resolution for the chosen gyro design.

The plots of $\frac{\partial \Omega}{\partial k_s}$, $\frac{\partial \Omega}{\partial m_d}$ and $\frac{\partial \Omega}{\partial m_s}$ with respect to the respective normalized design parameters also follow similar pattern.

The effect on resolution due to change in the sense damping coefficient (C_s) is given by Eq. (12). The same is plotted in Fig. 15. This plot also can be analysed in two regions. In region 1, there is a rapid variation in the slope of resolution with respect to change in C_s . This is the region of high sensitivity of gyro. For higher values of C_s (> 2.5 times the nominal value) represented by the region 2, the sensitivity reduces and hence resolution decreases almost linearly.

$$\frac{\partial(\Omega_{\min})}{\partial C_s} = \frac{-1}{S^2} \times \left(\frac{\Delta C_{\min} g_0^2}{2 \in_0 A} \right) \times \left(- \left[\frac{2A_d \omega_d^3 C_s}{m_s^2 \omega_s^6 \left[\left(\frac{\omega_d^2}{\omega_s^2} - 1 \right)^2 + \frac{\omega_d^2 C_s^2}{m_s^2 \omega_s^4} \right]^{\frac{3}{2}}} \right] \right) \quad (12)$$

4.5 Effect of variation in k_d , k_s , m_d , m_s and C_s on dynamic range

The dependence of the dynamic range on drive stiffness k_d , is studied using Eqs. (6) and (13)

$$\frac{\partial R}{\partial k_d} = \left(-\frac{20 \times \Omega_{\min} \left(\frac{1}{\Omega_{\min}} + \frac{\Omega_{\max} - \Omega_{\min}}{\Omega_{\min}^2} \right)}{\ln(10) \times (\Omega_{\max} - \Omega_{\min})} \right) \times \left(\frac{-1}{S^2} \times \left(\frac{\Delta C_{\min} s_0^2}{2 \in_0 A} \right) \times \left(\frac{1}{2 \times \sqrt{m_d k_d}} \times \left[\frac{2A_d}{\omega_s^2 \sqrt{\sigma_1}} - \left\{ \frac{A_d \omega_d \left[\frac{4\omega_d \left(\frac{\omega_d^2}{\omega_s^2} - 1 \right) + \frac{2\omega_d C_s^2}{m_s^2 \omega_s^4} \right]}{\omega_s^2 \sigma_1^{\frac{3}{2}}} \right\} \right] \right) \right) \right). \tag{13}$$

The plots of variation in dynamic range due to change in k_d , k_s , m_d , m_s and C_s are similar to those for scale factor variation. However, for large dynamic range, the maximum value of C_s is almost four times the nominal value increasing the design space with wider range of damping pressures.

5 Results and discussion

Table 5 provides the information on the sensitivity of each performance criterion against variation in each design parameter expressed in percentage. For example, for a 10% variation in drive stiffness, scale factor sensitivity is almost 100%, bandwidth sensitivity is around 5%, resolution sensitivity is almost double that of scale factor sensitivity and dynamic range sensitivity is around 90%. Tables 4 and 5 provide the necessary inputs to the designer as to which design parameter or geometric dimension needs to be changed to achieve the desired performance criteria. For achieving higher scale factor, high resolution and higher dynamic range, Table 5 shows that we can vary any of the variables k_d , k_s , m_d and m_s . However, Table 4 shows that maximum effect is obtained by changing k_s . There are two ways to change k_s as is evident from Table 4 and the maximum variation is obtained by changing the sense beam thickness (d_s). For larger bandwidth, or to separate the drive and sense

frequencies, Table 5 shows that the design parameters m_d and m_s can be varied. Further, from Table 4, it can be inferred that m_s has maximum influence and it can be varied by changing the size of the proof mass l_p .

The whole exercise of the sensitivity analysis is done to extract the crucial design parameters and the corresponding geometric dimensions to achieve a set of desired performance criteria of the MEMS gyroscope. We now demonstrate the utility of the obtained results on two design case studies: (1) SOI wafer with 40 μm device layer and (2) SOI wafer with 80 μm device layer.

Table 6 shows the targeted performance criteria of the MEMS gyroscope. Table 7 represents the design optimization done for a case in which an SOI wafer with 40 μm device layer is used. The target is to achieve almost the same or better performance specifications as mentioned in Table 6, with minimum changes in the geometric dimensions and also no change in the footprint of the sensor die. The first column of Table 7 represents the unmodified geometric dimensions (same dimensions as in the previous design), design parameters and performance criteria (changed as the structural thickness is reduced to 40 μm). From the values of the performance criteria obtained, we can see that the scale factor is less than desired, bandwidth is large, resolution is less and dynamic range is less compared to the targeted values. Using the knowledge from sensitivity analysis, the sense beam thickness (d_s) is decreased by

Table 5 Dependence of critical performance criteria on design parameters of the gyro

Design parameter being varied (nominal value ± 10%)	Maximum absolute variation in sensitivity of performance criteria (%)			
	Scale factor	Bandwidth	Resolution	Dynamic range
Drive stiffness (k_d)	99	5	213	87
Sense stiffness (k_s)	95	5	201	88
Drive mass (m_d)	99	17	213	88
Sense mass (m_s)	99	17	227	88
Damping pressure ($P_{damping}$)/sense damping coefficient (C_s)	3	0	2	2

Table 6 Targeted values of critical performance criteria of the MEMS gyroscope

Critical performance criteria	Value
Scale factor (S)	$> 100 \text{ aF}/(^{\circ}/\text{s})$
Bandwidth (BW)	25–35 Hz
Resolution (Ω_{min})	$< 0.01^{\circ}/\text{s}$
Dynamic range (R)	$> 90 \text{ dB}$

1 μm without touching any other geometric dimension. This situation is represented by the second column of Table 7. We can see that the sense frequency becomes lower than the drive frequency. This causes the sense mode to get excited before the drive mode and this case cannot be considered as normal operation of the gyro. In order to separate the frequencies and achieve a positive bandwidth, the sense mass (m_s) is reduced by reducing the proof mass size (l_p) by 20 μm while other dimensions are kept the same as before. This brings us to the region of the desired performance criteria as is clear from the third column of Table 7. Thus out of seven available geometric dimensions, only two were used in this case to achieve the desired results.

Table 8 represents the design optimization for a case in which an SOI wafer with 80 μm device layer is used. The targeted performance criteria are the same as mentioned in Table 6. From the values of the design parameters obtained for the unmodified case, we can see that the sense frequency is less than the drive frequency. As in the previous case, the frequencies are separated to get a positive bandwidth by reducing the sense mass (m_s) achieved by

reducing the size (l_p) by 100 μm while other dimensions are kept the same as before. This brings us to the region of the desired performance criteria as is clear from the second column of Table 8. Thus the fine tuning of the design is completed with just one modification to achieve the desired performance specifications.

These case studies prove that the technique of sensitivity analysis helps the designer in avoiding laborious simulations by varying different dimensions and thus keep on wandering in the huge design space for getting the desired results. Once the nominal values of the key geometric dimensions are known, they can be varied suitably to achieve the desired range of values for the performance criteria. It is worth pointing out that a serious design optimization tool will have the sensitivity analysis built into its algorithm for optimal-point search in the multidimensional design space. However, none of the existing MEMS design tools have such optimizer and hence the users generally tend to use ad-hoc approaches of trial and error to arrive at the final dimensions. The sensitivity analysis presented here provides a solid and reliable method for achieving the target specifications with minimum design iterations.

6 Conclusion

The complete design and simulation of a high performance MEMS gyroscope to meet all the important performance specifications is presented in this paper. This is followed by a comprehensive sensitivity analysis that provides the

Table 7 Design optimization for case study 1—SOI with 40 μm device layer

	Unmodified	Modification 1	Modification 2
Geometric dimensions (μm)	$l_d = 700$	$l_d = 700$	$l_d = 700$
	$w_d = 8$	$w_d = 8$	$w_d = 8$
	$d_s = 8$	$d_s = 7$	$d_s = 7$
	$w_s = 11$	$w_s = 11$	$w_s = 11$
	$w_f = 200$	$w_f = 200$	$w_f = 200$
	$l_p = 500$	$l_p = 500$	$l_p = 480$
	$P_{damping} = 1 \text{ mbar}$	$P_{damping} = 1 \text{ mbar}$	$P_{damping} = 1 \text{ mbar}$
Design parameters	$k_d = 24.71 \text{ N/m}$	$k_d = 7.55 \text{ N/m}$	$k_d = 24.63 \text{ N/m}$
	$k_s = 10.99 \text{ N/m}$	$k_s = 24.63 \text{ N/m}$	$k_s = 7.57 \text{ N/m}$
	$m_d = 5.24 \times 10^{-8} \text{ kg}$	$m_d = 1.62 \times 10^{-8} \text{ kg}$	$m_d = 5.14 \times 10^{-8} \text{ kg}$
	$m_s = 1.63 \times 10^{-8} \text{ kg}$	$m_s = 5.22 \times 10^{-8} \text{ kg}$	$m_s = 1.54 \times 10^{-8} \text{ kg}$
	$C_s = 3.33 \times 10^{-6} \text{ N}/(\text{m/s})$ ($f_s = 4133 \text{ Hz} > f_d = 3456 \text{ Hz}$)	$C_s = 3.33 \times 10^{-6} \text{ N}/(\text{m/s})$ ($f_s = 3437 \text{ Hz} < f_d = 3457 \text{ Hz}$)	$C_s = 3.22 \times 10^{-6} \text{ N}/(\text{m/s})$ ($f_s = 3528 \text{ Hz} > f_d = 3484 \text{ Hz}$)
	Performance criteria	$S = 8.13 \text{ aF}/(^{\circ}/\text{s})$	Cannot be computed as $f_s < f_d$
$BW = 367 \text{ Hz}$			$BW = 34 \text{ Hz}$
$\Omega_{min} = 0.102^{\circ}/\text{s}$			$\Omega_{min} = 0.0065^{\circ}/\text{s}$
$R = 72 \text{ dB}$			$R = 96 \text{ dB}$

Table 8 Design optimization for case study 2—SOI with 80 μm device layer

	Unmodified	Modification 1
Geometric dimensions (μm)	$l_d = 700$ $w_d = 8$ $d_s = 8$ $w_s = 11$ $w_f = 200$ $l_p = 500$ $P_{damping} = 1 \text{ mbar}$	$l_d = 700$ $w_d = 8$ $d_s = 8$ $w_s = 11$ $w_f = 200$ $l_p = 400$ $P_{damping} = 1 \text{ mbar}$
Design parameters	$k_d = 54.31 \text{ N/m}$ $k_s = 11.42 \text{ N/m}$ $m_d = 1 \times 10^{-7} \text{ kg}$ $m_s = 3.22 \times 10^{-8} \text{ kg}$ $C_s = 3.33 \times 10^{-6} \text{ N/(m/s)}$ $(f_s = 2997 \text{ Hz} < f_d = 3448 \text{ Hz})$	$k_d = 47.75 \text{ N/m}$ $k_s = 11.4 \text{ N/m}$ $m_d = 9.04 \times 10^{-8} \text{ kg}$ $m_s = 2.1 \times 10^{-8} \text{ kg}$ $C_s = 2.272 \times 10^{-6} \text{ N/(m/s)}$ $(f_s = 3709 \text{ Hz} > f_d = 3658 \text{ Hz})$
Performance criteria	Cannot be computed as $f_s < f_d$	$S = 108.94 \text{ aF}/(^{\circ}/\text{s})$ $BW = 29 \text{ Hz}$ $\Omega_{min} = 0.007^{\circ}/\text{s}$ $R = 95 \text{ dB}$

crucial understanding of the change in different performance criteria with change in design parameters. The influence of variation in various geometric dimensions of the structure on the design parameters of the gyro is established. The critical geometric dimensions are identified that are suitably modified allowing faster convergence of the design to the range of desired performance specifications. In our two case studies, the maximum number of design iterations required to achieve the targeted specifications from the chosen initial structural thickness is only 2. While this may not be the case for all designs, the number of iterations required will be certainly low. This study is relevant on two counts (1) the fine tuning of the design to meet all the desired performance criteria with minimum variation in geometric dimensions and with no change in the footprint of the sensor die and (2) the influence of geometric dimensional variations induced during the fabrication of the MEMS gyro structure. The same technique can be extended to other type of MEMS gyroscope design as well and the principle can be used with appropriate set of parameters to any MEMS design.

References

- Acar C, Shkel AM (2005) An approach for increasing drive-mode bandwidth of MEMS vibratory gyroscopes. *JMEMS* 14(3):520–528
- Acar C, Shkel A (2009) MEMS vibratory gyroscopes—structural approaches to improve robustness. Springer, ISBN 978-0-387-09535-6
- Adamst S, Grovest J, Shawt K, Davist T, Cardareli D, Carroll R, Walsh J, Fontanella M (1999) A single-crystal silicon gyroscope with decoupled drive and sense. *SPIE* 3876:74–83
- Alper SE, Azgin K, Akin T (2007) A high-performance silicon-on-insulator MEMS gyroscope operating at atmospheric pressure. *Sens Actuators A* 135:34–42
- Apostolyuk V (2006) Theory and design of micromechanical vibratory gyroscopes. *MEMS/NEMS handbook—techniques and applications*, pp 173–195
- Bao M-H (2000) Micromachined transducers – pressure sensors, accelerometers and gyroscopes. *Handbook of sensors and actuators*, p 8
- Bernstein J, Cho S, King AT, Kourepenis A, Maciel P, Weinberg M (1993) A micromachined comb-drive tuning fork rate gyroscope. *IEEE*, pp 143–148
- Blom FR, Bouwstra S, Elwenspoek M, Fluitman JHJ (1992) Dependence of the quality factor of micromachined silicon beam resonators on pressure and geometry. *J Vac Sci Technol* 10:19–26
- Chang H, Zhang Y, Xie J, Zhou Z, Yuan W (2010) Integrated behavior simulation and verification for a MEMS vibratory gyroscope using parametric model order reduction. *JMEMS* 19(2):282–293
- Coventor Inc (2015) Coventorware analyzer version 10 field solver reference
- Dong H, Xiong X (2009) Design and analysis of a MEMS comb vibratory gyroscope, UB-NE ASEE 2009 conference
- Ferguson MI, Keymeulen D, Peay C, Yee K (2005) Effect of temperature on MEMS vibratory rate gyroscope. *IEEE*, pp 1–6
- Geiger W, Folkmer B, Merz J, Sandmaier H, Lang W (1999) A new silicon rate gyroscope. *Sens Actuators* 73:45–51
- Hopcroft MA, Nix WD, Kenny TW (2010) What is the Young's modulus of silicon? *JMEMS* 19(2):229–238
- Kawai H, Atsuchi K-I, Tamura M, Ohwada K (2001) High-resolution microgyroscope using vibratory motion adjustment technology. *Sens Actuators A* 90:153–159
- Mochida Y, Tamura M, Ohwada K (2000) A micromachined vibrating rate gyroscope with independent beams for the drive and detection modes. *Sens Actuators* 80:170–178

- Park KY, Lee CW, Oh YS, Cho YH (1997) Laterally oscillated and force-balanced micro vibratory rate gyroscope supported by fish hook shape springs. *IEEE*, pp 494–499
- Prikhodko IP, Zotov SA, Trusov AA, Shkel AM (2011) sub-degree-per-hour silicon MEMS rate sensor with 1 million Q-factor. *IEEE*, pp 2809–2812
- Senturia SD (2001) *Microsystem design*. Kluwer, Boston
- Sharma A, Zaman MF, Zucher M, Ayazi F (2008) A 0.1°/hr bias drift electronically matched tuning fork microgyroscope. *IEEE*, pp 6–9
- Tanaka K, Mochida Y, Sugimoto M, Moriya K, Hasegawa T, Atsuchi K, Ohwada K (1995) A micromachined vibrating gyroscope. *Sens Actuators A* 50:111–115
- Tatar E, Alper SE, Akin T (2012) Quadrature-error compensation and corresponding effects on the performance of fully decoupled MEMS gyroscopes. *JMEMS* 21(3):656–667
- Tatar E, Mukherjee T, Fedder GK (2014) Simulation of stress effects on mode-matched MEMS gyroscope bias and scale factor. *IEEE*, pp 16–20
- Trusov AA et al (2010) Micromachined rate gyroscope architecture with ultra-high quality factor and improved mode ordering. *Sens Actuators A Phys*. <https://doi.org/10.1016/j.sna.2010.01.007>
- Weber M, Bellrichard M, Kennedy C (2004) High angular rate and high G effects in the MEMS gyro. Coventor website (**online**)
- Yoon S, Park U, Rhim J, Yang SS (2015) Tactical grade MEMS vibrating ring gyroscope with high shock reliability. *Microelectron Eng* 142:22–29